Low-Temperature Solution-Processed Perovskite Solar Cells with High Efficiency and Flexibility

Jingbi You,[†] Ziruo Hong,[†,*] Yang (Michael) Yang,[†] Qi Chen,[†] Min Cai,[†] Tze-Bin Song,[†] Chun-Chao Chen,[†] Shirong Lu,[†] Yongsheng Liu,[†] Huanping Zhou,[†,*] and Yang Yang[†,‡,*]

[†]Department of Materials Science and Engineering and [‡]California NanoSystems Institute, University of California—Los Angeles, Los Angeles, California 90095, United States

ABSTRACT Perovskite compounds have attracted recently great attention in photovoltaic research. The devices are typically fabricated using condensed or mesoporous TiO_2 as the electron transport layer and 2,2′7,7′-tetrakis-(*N*,*N*-dip-methoxyphenylamine)9,9′-spirobifluorene as the hole transport layer. However, the high-temperature processing (450 °C) requirement of the TiO_2 layer could hinder the widespread adoption of the technology. In this report, we adopted a low-temperature processing technique to attain high-efficiency devices in both rigid and flexible substrates, using device structure substrate/ITO/PEDOT:PSS/$CH_3NH_3PbI_{3-x}Cl_x$/PCBM/Al, where PEDOT:PSS and PCBM are used as hole and electron transport layers, respectively. Mixed halide perovskite, $CH_3NH_3PbI_{3-x}Cl_x$, was used due to its long carrier lifetime and good electrical properties. All of these layers are solution-processed under 120 °C. Based on the proposed device structure, power conversion efficiency (PCE) of 11.5% is obtained in rigid substrates (glass/ITO), and a 9.2% PCE is achieved for a polyethylene terephthalate/ITO flexible substrate.

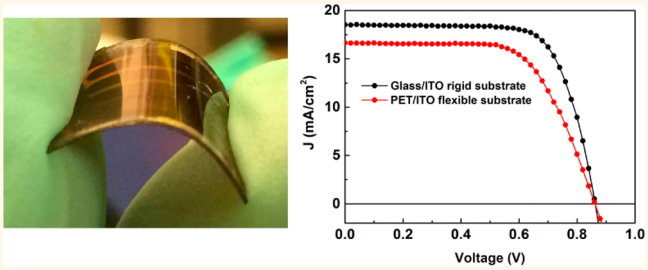

KEYWORDS: perovskite solar cells · low temperature · planar structure · flexible solar cells

Perovskite semiconductors have attracted tremendous attention[1,2] beginning with their incorporation into photovoltaic devices by Miyasaka *et al.* in 2009,[3] achieving an initial power conversion efficiency (PCE) of 4%. In 2012, significant progress was realized in perovskite solar cells, with several groups reporting over 10% PCE by employing mesoporous nanostructures,[4−10] attracting great attention in the field of photovoltaics.[11−16] More recently, it was observed that perovskite materials exhibit long charge carrier lifetimes and thus can be used for planar junctions.[17,18] In fact, both the solution and coevaporation processing approaches showed up to a 11.4[19] and 15%[20] PCE, respectively, incorporating a planar structure. However, it has been recognized that, in the perovskite-based photovoltaic cells, a high-quality condensed TiO_2 layer often requires high-temperature treatment above 450 °C. Such extreme processing conditions could limit the future development of perovskite solar cells, particularly in flexible formats. It is therefore critical to explore the possibility of fabricating high-performance perovskite-based solar cells at low temperature. In addition, a low-temperature processing approach offers a wider selection of potential substrates and electrode materials that could be used in devices, including polymer-based flexible substrates and solution-processed interfacial materials that could thereby be incorporated into perovskite photovoltaic cells. A few groups have attempted to fabricate all low-temperature processed perovskite solar cells using different transport layer processing.[21−23] However, the resultant device efficiency is notably inferior compared to high-temperature processed TiO_2. The efficiency losses in the low-temperature processed perovskite solar cells originate mainly due to charge recombination at imperfect interfaces and structural or chemical defects in perovskite films.

In this article, we explore the possibility of fabricating perovskite-based solar cells *via* a low-temperature (<120 °C) solution-processing approach. We obtain 11.5% PCE based on a glass/ITO rigid substrate, which is

* Address correspondence to yangy@ucla.edu, zrhong@ucla.edu, happyzhou@ucla.edu.

Received for review November 21, 2013 and accepted January 5, 2014.

Published online January 05, 2014
10.1021/nn406020d

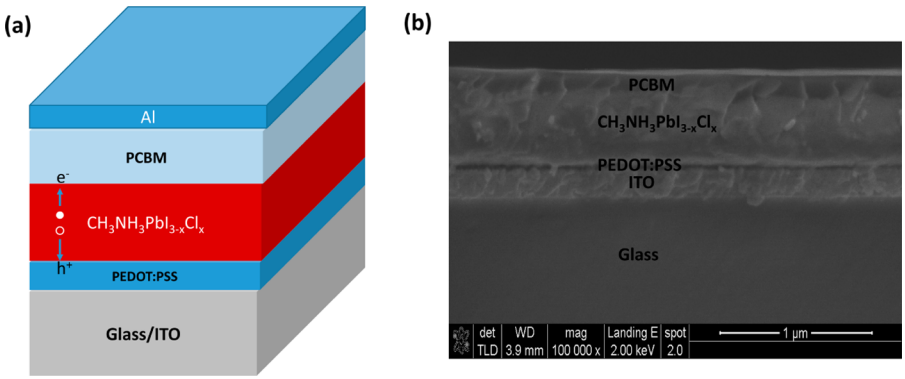

Figure 1. Device structure of low-temperature processed perovskite solar cells. From the bottom: glass/ITO/PEDOT:PSS/$CH_3NH_3PbI_{3-x}Cl_x$/PCBM/Al. The cross section of the device except for the Al electrode. The thicknesses of PEDOT:PSS, perovskite absorbing layer, and PCBM layers are 40, 340, and 110 nm, respectively.

comparable to what is obtained with high-temperature approaches. For the polyethylene terephthalate (PET)/ITO flexible substrates, over 9% PCE has been demonstrated. In addition, we have studied the charge transport properties between perovskite and n/p buffer layer and also investigated the materials properties of $CH_3NH_3PbI_{3-x}Cl_x$.

RESULTS AND DISCUSSION

The device structure is shown in Figure 1a (starting from the bottom: glass/ITO substrate, hole transport layer PEDOT:PSS, perovskite photoactive layer, and PCBM electron transport layer, with a final Al electrode deposited *via* thermal evaporation). The top-view and cross-section scanning electron microscopy (SEM) images of the $CH_3NH_3PbI_{3-x}Cl_x$ film on the PEDOT:PSS layer are shown in Supporting Information Figure SI-1. The results reveal that the perovskite film is uniform despite some pinholes, and after coating PCBM on the top of the perovskite layer, the surface appears smooth and fully covered by PCBM, which is shown in the top-view SEM images in Figure SI-2. The cross-section SEM images of devices without the Al electrode shown in Figure 1b show a well-defined layer-by-layer structure with sharp interfaces. The thicknesses of the PEDOT:PSS, perovskite, and PCBM layers are 40, 340, and 110 nm, respectively. Here, the thickness of the $CH_3NH_3PbI_{3-x}Cl_x$ layer is sufficient to serve as the light-absorbing layer. Moreover, charge extraction from the photoactive layer is still efficient due to the long carrier lifetime and good carrier transport properties. For the same reason, the perovskite layer used here, $CH_3NH_3PbI_{3-x}Cl_x$, is allowed to be much thicker than previously reported $CH_3NH_3PbI_3$ thicknesses,[22] ensuring sufficient light absorption, which is the first decisive factor for optimal device performance.

The X-ray diffraction (XRD) pattern of $CH_3NH_3PbI_{3-x}Cl_x$ is shown in Figure SI-2, where the perovskite material without Cl^- anions ($CH_3NH_3PbI_3$) is compared with the $CH_3NH_3PbI_{3-x}Cl_x$ investigated herein. It was found that the XRD patterns of the two materials are almost identical, suggesting that the Cl^- anion does not alter the crystalline structure. In addition, the film is highly orientated along the (110) direction.[8] Considering the similar diffraction patterns of $CH_3NH_3PbI_{3-x}Cl_x$ and $CH_3NH_3PbI_3$, it strongly suggests that only a little Cl has been incorporated into the perovskite materials.

To investigate the atomic ratios in $CH_3NH_3PbI_{3-x}Cl_x$, especially of I and Cl, X-ray photoelectron spectroscopy (XPS) measurements were performed. The full XPS spectra of the materials are shown in Figure 2a, and the I 3d and Cl 2p core energy level spectra are shown in Figure 2b,c, respectively. It can be calculated that Cl/(Cl + I) is 2.2% in $CH_3NH_3PbI_{3-x}Cl_x$, which is surprisingly small and much lower than the composition stoichiometry in the precursor solution. We have measured the Cl in several samples from the same batch, and all of the results showed that the amount of Cl in $CH_3NH_3PbI_{3-x}Cl_x$ is very small or under the limitation of the XPS instrument. Even though Cl^- anions play important roles in perovskite compounds in the dynamics of excitons and/or charge carrier transport. Literature shows that Cl content improves the lifetime and/or enhances the charge mobility of perovskite materials;[19] however, the underlying mechanism on why Cl plays a positive role in the photovoltaic cells remains unclear. To investigate charge carrier (or excitons) behavior in $CH_3NH_3PbI_{3-x}Cl_x$ films, we measured the valence band maximum (VBM, distance from valence band to Fermi level)[24] as shown in Figure 2d. The energy difference between the Fermi level and the valence band edge is about 1.1 eV, with the band gap of perovskite material approximately 1.5 eV[7] (the band gap value is estimated from the absorption band edge of the perovskite film in Figure SI-4). Therefore, the Fermi level of the perovskite film lies closer to the conduction band edge than that of the valence band edge, indicating that the perovskite is a weak n-type or intrinsic semiconductor. Etgar *et al.* have reported that $CH_3NH_3PbI_3$ shows a p-type behavior.[25] These results are very interesting and different from our present

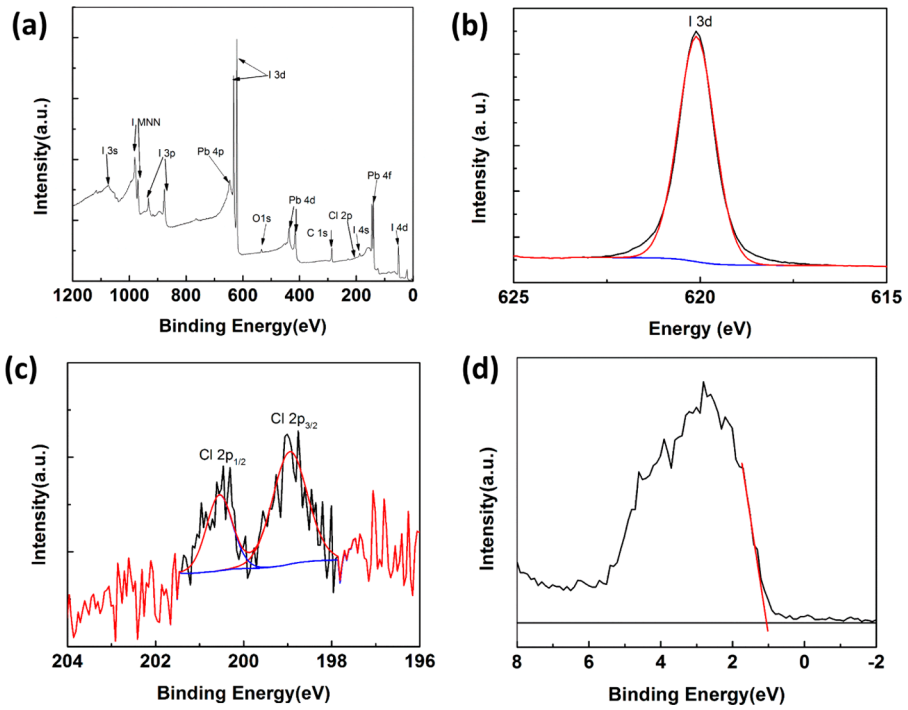

Figure 2. (a) X-ray photoelectron spectroscopy (XPS) of the $CH_3NH_3PbI_{3-x}Cl_x$, (b) XPS spectra of I 3d, (c) XPS spectra of Cl 2p including Cl $2p_{1/2}$ and Cl $2p_{3/2}$, (d) valence band of $CH_3NH_3PbI_{3-x}Cl_x$; the Fermi level is located at 0 eV.

results, which may be from different experimental conditions, indicating that the perovskite material properties could be tuned by processing parameters.

Because the electrical buffer layers, PEDOT:PSS as hole transport layer and PCBM as electron transport layer, can extract free carriers and dissociate excitons into free charges, we measure charge generation of the perovskite photovoltaic cells *via* photoluminescence (PL) and time-resolved photoluminescence (TRPL) characterization. The PL of $CH_3NH_3PbI_{3-x}Cl_x$, PEDOT:PSS/$CH_3NH_3PbI_{3-x}Cl_x$, $CH_3NH_3PbI_{3-x}Cl_x$/PCBM, and PEDOT:PSS/$CH_3NH_3PbI_{3-x}Cl_x$/PCBM on glass substrates was measured. The excitation light enters the sample from the glass substrate side with an incidental angle of 30°, and PL emission is collected from the glass substrate side, as well. From the PL data, we observed a significant quenching effect when the pevoskite layer establishes contact with either the PEDOT:PSS or the PCBM layer. The PCBM-coated perovskite film shows completely quenched PL, and the PEDOT:PSS-based sample exhibits roughly 10% PL, indicating that charge generation is possible at both interfaces, with carrier generation at the perovskite/PEDOT:PSS interface slightly less than the perovskite/PCBM interface. (It has to be mentioned that the different substrate might also affect the growth of perovskite. Thus, glass or glass coated with PEDOT:PSS layer substrates could lead to different PL behavior. Therefore, the PL quench behavior between PEDOT:PSS and the perovskite layer is hard to accurately define.) To further confirm these charge transport processes, the time-resolved photoluminescence has been measured and is shown in Figure 3b. Fitting the data with two exponential decay curves (here, the longer lifetime was used for comparison) yields the lifetime of carriers and/or excitons. For the perovskite neat film, a PL lifetime as high as 200.1 ns was observed, consistent with previous reports,[18] the long lifetime is tentatively ascribed to the Cl doping effect.[18] This long lifetime is essential for longer exciton/carrier diffusion lengths to allow large film thicknesses for light harvesting. When the perovskite film forms a contact with PEDOT:PSS or PCBM, it was observed that the PL lifetime is reduced significantly. For the PEDOT:PSS case, the lifetime decreases to 50 ns, and when coating the PCBM layer on the perovskite layer, the carrier lifetime further drops to 25.4 ns, indicating that charge transfer from perovskite to PCBM could be faster than that of the PEDOT:PSS. Considering the strong quenching effect of PEDOT:PSS and PCBM to the PL emission from the perovskite layer, the PL lifetime of the PEDOT:PSS/perovskite layer/PCBM further decreases to 18 ns. We propose that the PL quenching is caused by fast charge transfer at the interface, which may be the mechanism of charge separation and collection in these devices.

Figure 4a shows the device performance of the control device using the device structure ITO/PEDOT:PSS/perovskite/PCBM layer. Specifically, the open circuit voltage (V_{OC}) is 0.87 V, the short circuit current (J_{SC}) is 18.5 mA/cm^2, and filling factor (FF) is 72% with 11.5% power conversion efficiency based on the employed simple device structure. In addition, we noticed that our devices exhibit high reproducibility, with the

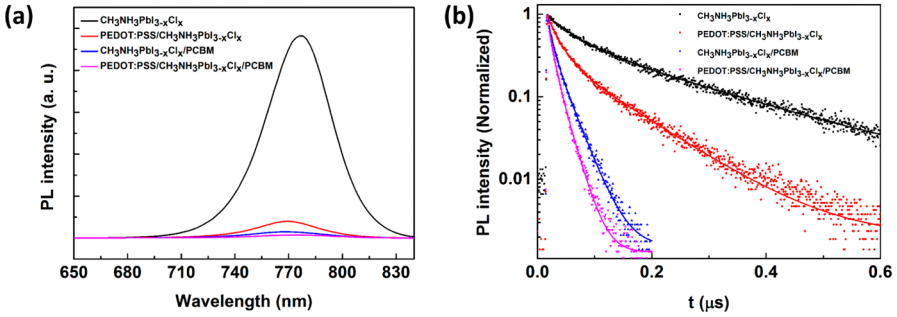

Figure 3. (a) Photoluminescence of $CH_3NH_3PbI_{3-x}Cl_x$, PEDOT:PSS/$CH_3NH_3PbI_{3-x}Cl_x$, $CH_3NH_3PbI_{3-x}Cl_x$/PCBM, and PEDOT:PSS/$CH_3NH_3PbI_{3-x}Cl_x$/PCBM on glass substrate. (b) Time-resolved photoluminescence of $CH_3NH_3PbI_{3-x}Cl_x$, PEDOT:PSS/$CH_3NH_3PbI_{3-x}Cl_x$, $CH_3NH_3PbI_{3-x}Cl_x$/PCBM, and PEDOT:PSS/$CH_3NH_3PbI_{3-x}Cl_x$/PCBM. Symbols are measurement results; solid lines are two exponential fits.

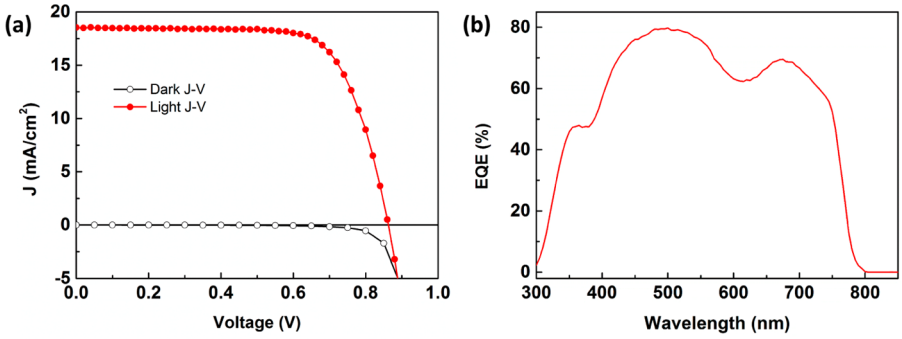

Figure 4. (a) $J-V$ curve of the devices on rigid glass/ITO substrate under 1 sun illumination (100 mW/cm^2). The dark curve of the device is also included. (b) External quantum efficiency of the devicesp; the integrated short circuit current is 17.2 mA/cm^2.

average efficiency of the devices being above 10%, with the V_{OC} ranging from 0.80 to 0.88 V, the J_{SC} varies from 16.5 to 19 mA/cm^2, and the FF ranges from 65 to 74%. These are the best results based on fully low-temperature processed devices. The photovoltaic performance is directly related to good morphology, long carrier lifetime, and enhanced charge transport properties. It is worth mentioning that the thickness of PCBM is very critical for achieving high performance. On one hand, if the PCBM layer is too thin, it will not fully cover the perovskite layer, the electrode layer, for example, Al, will directly contact with perovskite layer; on the other hand, if the PCBM is too thick, the series resistance of the device will be increased due to the low conductivity of PCBM. Both of them will lead to inferior device performance.

Compared to previous results based on $CH_3NH_3PbI_{3-x}Cl_x$ fabricated through evaporation,[20] our devices showed comparable short circuit currents, as well as high filling factors, indicating that the hole −electron transport balance is close to perfect. With the highest V_{OC} for perovskite solar cells reaching above 1 V,[8,20] our device demonstrated the V_{OC} around 0.84 ± 0.04 V. This difference could be due to the voids in the perovskite layer, causing leakage current and induced recombination. These issues can be further addressed with improved morphology, possibly reaching power conversion efficiencies above 12%. Moreover, the contact between the perovskite and buffer layers could be further improved by choosing materials with suitable energy levels to the perovskite layer. In addition to using PCBM as an electron transport layer (ETL), ZnO was also tested as the electron transport layer[26] in low-temperature processed perovskite solar cells. The device performance using PCBM and ZnO showed similar device performance ($J-V$ curve of the devices using ZnO as ETL is shown in Figure SI-5). The external quantum efficiency for the device achieving 11.5% PCE is shown in Figure 4b. The device showed high external quantum efficiency, peaking close to 80%. The integrated short circuit current based on EQE is 17.2 mA/cm^2, which is consistent with results obtained from solar simulators. Compared to similar structures using $CH_3NH_3PbI_3$,[22,23] the short circuit current was found to range from 10 to 18 mA/cm^2, where the improvement mainly arises from the increased thickness of the perovskite layer; hence, the device benefits from the long lifetime and good charge transport properties of $CH_3NH_3PbI_{3-x}Cl_x$. The external quantum efficiency of this device could be further improved by optical engineering such as light trapping[27] or plasmonic effects.[28−30]

To investigate charge recombination in low-temperature processed perovskite solar cells, light intensity dependence was measured. Figure 5a shows the $J-V$ curve under different light intensities ranging

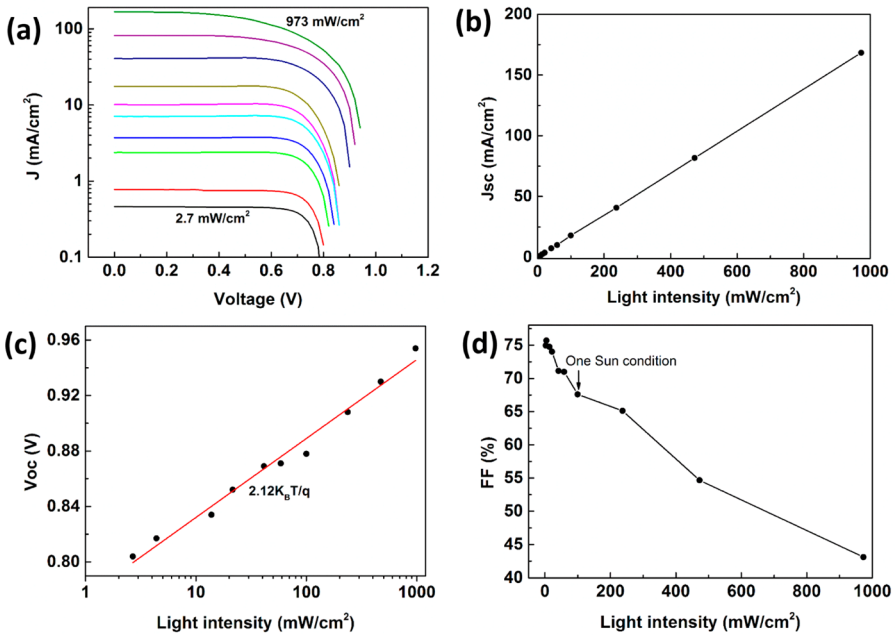

Figure 5. (a) $J-V$ curve of the perovskite solar cells under different light intensity (I) from 2.7 to 973 mW/cm^2 (0.027−9.73 sun). (b−d) Variation of short circuit current (J_{SC}), open circuit voltage (V_{OC}), and the $\delta V_{OC} \sim \ln(I)$ fitted by a linear relationship; the slope is $2.12k_BT/q$, FF of the typical perovskite device under different light intensity from 2.7 to 973 mW/cm^2.

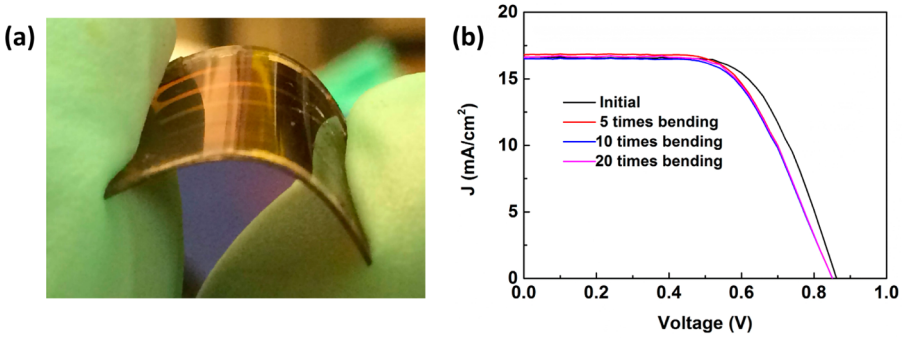

Figure 6. (a) Photo image of flexible perovskite solar cells on PET/ITO substrate, and (b) device performance of the perovskite solar cells on PET/ITO flexible substrate before and after bending.

from 0.027 to 9.73 sun. The corresponding photovoltaic parameters such as J_{SC}, V_{OC}, and FF dependence on the light intensity are plotted in Figure 5b−d, respectively. Results show that J_{SC} is linear with light intensity, indicating no significant energy barrier in the devices. From the relationship between $\delta V_{OC} \sim \ln(I)$, the slope of the fitting curve is 0.056, close to 0.052 ($2k_BT/q$), indicating that the main recombination mechanism in the devices is free carrier recombination.[31] The FF is 43% at about 10 sun illumination and can be as high as 75% under low light intensity (~0.1 sun), indicating reduced recombination due to the decrease of free charge carrier concentration.[32] The power conversion efficiency dependence on light intensity is shown in Figure SI-6. Results show that the power conversion efficiency of the devices can be increased from 10.4 to 10.9%. (It should be noted that the device used for the light-dependent measurement is not our best device.) The original photovoltaic parameters are V_{OC} = 0.88 V, J_{SC} = 17.5 mA/cm^2, FF = 67.6%, and PCE = 10.4%.

We have achieved high device performance based on low-temperature (less than 120 °C) solution-processed perovskite solar cells, suggesting that it is also possible to attain high device performance of flexible solar cells based on the processing techniques utilized. Here, we replaced the rigid glass/ITO substrate with a flexible PET/ITO substrate and fabricated the devices *via* the same procedures. A photograph of the flexible device is shown in Figure 6a. The flexible device shows V_{OC} of 0.86 V, J_{SC} of 16.5 mA/cm^2, and FF of 64%. Furthermore, power conversion efficiency of 9.2% is achieved, keeping 80% of the rigid devices' performance. In comparison with the rigid devices, the loss in PCE arises from the decreased J_{SC} and FF, which could be due to the higher series resistance of the flexible devices, issues that could be solved in the near future. For the flexible structure, we also tested the

effects of mechanical bending on device performance; the devices' performance after bending is also included in Figure 6b. Results show that the device maintains its performance through mechanical bending up to 20 times, indicating that our devices tolerate repeated mechanical deformation.

CONCLUSIONS AND PROSPECTS

In conclusion, we have demonstrated low-temperature solution-processed perovskite solar cells. The device performance achieved is comparable to that found for conventional high-temperature processing approaches. We achieved 11.5% power conversion efficiency in a rigid substrate devices and a 9.2% efficiency in flexible devices based on this processing approach. The imperfection in the morphology of the perovskite layer induces recombination and V_{OC} loss. Further improvements could be achieved by fine-tuning the layer morphology. In organic solar cell areas, annealing,[33] slow growth,[34] additive,[35] and other approaches have been successfully used to tune the morphology. We think we can borrow these ideas and apply it into perovskite solar cells research area.

EXPERIMENTAL SECTION

Materials and Characterizations. $PbCl_2$ was purchased from Alfa Aesar. The material CH_3NH_3I was synthesized in our lab using the approach outlined in ref 36. PEDOT:PSS and PCBM were purchased from Clevious and Nano-C, respectively. ZnO was synthesized based on the recipe in ref 26. The ZnO nanoparticles were synthesized in methanol and redispersed in 3 wt % chlorobenzene. The X-ray diffraction patterns were collected on a PANalytical X'Pert Pro X-ray powder diffractometer using Cu Kα radiation ($\lambda = 1.54050$A). The scanning electron microscope images were taken on a JEOL JSM-6700F. Steady-state photoluminescence was measured by Horiba Jobin Yvon system with an excitation at 600 nm. In the time-resolved photoluminescence measurement, the samples were excited by a pulsed laser (PDL 800-B system with an extended trigger) with a wavelength and frequency of 632 nm and 1 MHz, respectively. The PL photons were counted by Picoharp 300 after preamplification by PAM 102. (It has to be mentioned that the perovskite samples for photoluminescence were prepared in air environment). X-ray photoelectron spectroscopy was carried out in Kratos DLD XPS system. For XPS measurement, due to some charge effect, we use C 1s for calibration.

Device Fabrication and Measurement. PEDOT:PSS was spin-coated on an ITO surface under 4000 rpm and then annealed at 120 °C for 15 min. For the perovskite layer, a 1:3 ratio of $PbCl_2$/CH_3NH_3I was mixed. Specifically, the concentration of the $PbCl_2$ and CH_3NH_3I were 0.8 and 2.4 M. The solution was spin-coated onto the PEDOT:PSS layer at 1500 rpm and then annealed at 90 °C for 2 h. After that, 2% PCBM in chlorobenzene solution was coated onto the perovskite layer at 1000 rpm. Finally, the device was transferred to a vacuum chamber for Al electrode evaporation. Glass/ITO and PET/ITO substrates were used for rigid and flexible devices. The device area is 0.1 cm^2. $J-V$ characteristics of photovoltaic cells were taken using a Keithley 2400 source measure unit under a simulated AM1.5G spectrum. With an Oriel 9600 solar simulator, the light intensity was calibrated by KG-5 Si diode. External quantum efficiencies were measured by an Enli Technology (Taiwan) EQE measurement system. For the different light intensity response measurement, neutral density filters and aperture size were used to tune the light intensity, and a Si diode was used to calibrate the light intensity.

Conflict of Interest: The authors declare no competing financial interest.

Note added IN PROOF: During the revision of this paper, two highly relevant articles on this topic were published: Docampo, P.; Ball, J. M.; Darwich, M.; Eperon, G. E.; Snaith, H. J. Efficient organometal trihalide perovskite planar-heterojunction solar cells on flexible polymer substrates. *Nat. Commun.* **2013**, *4*, 2761. Malinkiewicz, O.; Yella, A.; Lee, Y. H.; Espallargas, G. M.; Graetzel, M.; Nazeeruddin, M. K.; Bolink, H. J. Perovskite solar cells employing organic charge-transport layers. *Nat. Photonics*, **2013**, DOI: 10.1038/nphoton.2013.341.

Acknowledgment. This work was financially supported by the Air Force Office of Scientific Research (AFOSR, Grant No. FA9550-09-1-0610), National Science Foundation (NSF ECCS-1202231), and UCLA internal funds. The authors would like to thank Mr. Shenglin Ye for XPS measurement, and Mr. Ding-Wen Chung and Miss Renee Green for proof reading.

Supporting Information Available: SEM images of perovskite film before and after coating PCBM layer, XRD of $CH_3NH_3PbI_{3-x}Cl_x$ and $CH_3NH_3PbI_3$, absorption of $CH_3NH_3PbI_{3-x}Cl_x$ with and without PCBM layer, $J-V$ curve of the low-temperature processed perovskite solar cells with glass/ITO/PEDOT:PSS/$CH_3NH_3PbI_{3-x}Cl_x$/ZnO/Al, and the relationship between power conversion efficiency with light intensity. This material is available free of charge *via* the Internet at http://pubs.acs.org.

REFERENCES AND NOTES

1. Kagan, C. R.; Mitzi, D. B.; Dimitrakopoulos, C. D. Organic–Inorganic Hybrid Materials as Semiconducting Channels in Thin-Film Field-Effect Transistors. *Science* **1999**, *286*, 945–947.
2. Liang, K.; Mitzi, D. B.; Prikas, M. T. Synthesis and Characterization of Organic–Inorganic Perovskite Thin Films Prepared Using a Versatile Two-Step Dipping Technique. *Chem. Mater.* **1998**, *10*, 403–411.
3. Kojima, A.; Teshima, K.; Shirai, Y.; Miyasaka, T. Organometal Halide Perovskites as Visible-Light Sensitizers for Photovoltaic Cells. *J. Am. Chem. Soc.* **2009**, *131*, 6050–6051.
4. Im, J.-H.; Lee, C. R.; Lee, J. W.; Park, S. W.; Park, N. G. 6.5% Efficient Perovskite Quantum-Dot-Sensitized Solar Cell. *Nanoscale* **2011**, *3*, 4088–4093.
5. Etgar, L.; Gao, P.; Xue, Z. S.; Peng, Q.; Chandiran, A. K.; Liu, B.; Nazeeuddin, M.; Graztel, M. Mesoscopic $CH_3NH_3PbI_3/TiO_2$ Heterojunction Solar Cells. *J. Am. Chem. Soc.* **2012**, *134*, 17396–17399.
6. Lee, M. M.; Teuscher, J.; Miyasaka, T.; Murakami, T. N.; Snaith, H. J. Efficient Hybrid Solar Cells Based on Meso-Superstructured Organometal Halide Perovskites. *Science* **2012**, *338*, 643–647.
7. Kim, H. S.; Lee, C. R.; Im, J. H.; Lee, K. B.; Moehl, T.; Marchioro, A.; Moon, S.; Humphry-Baker, R.; Yum, J. H.; Moser, J. E.; *et al.* Lead Iodide Perovskite Sensitized All-Solid-State Submicron Thin Film Mesoscopic Solar Cell with Efficiency Exceeding 9%. *Sci. Rep.* **2012**, *2*, 591.
8. Burschka, J.; Pellet, N.; Moon, S. J.; Humphry-Baker, R.; Gao, P.; Nazeeruddin, M. K.; Gratzel, M. Sequential Deposition as a Route to High-Performance Perovskite-Sensitized Solar Cells. *Nature* **2013**, *499*, 316–319.
9. Heo, J. H.; Im, S. H.; Noh, J. H.; Mandal, T. N.; Lim, C. S.; Chang, J. A.; Lee, Y. H.; Kim, H. J.; Sarkar, A.; Nazeeruddin, M. K.; *et al.* Efficient Inorganic–Organic Hybrid Heterojunction Solar Cells Containing Perovskite Compound and Polymeric Hole Conductors. *Nat. Photonics* **2013**, *7*, 486–492.
10. Noh, J. H.; Im, S. H.; Heo, J. H.; Mandal, T. N.; Seok, S. I. Chemical Management for Colorful, Efficient, and Stable Inorganic–Organic Hybrid Nanostructured Solar Cells. *Nano Lett.* **2013**, *13*, 1764–1769.

11. Park, N.-G. Organometal Perovskite Light Absorbers toward a 20% Efficiency Low-Cost Solid-State Mesoscopic Solar Cell. *J. Phys. Chem. Lett.* **2013**, *4*, 2423–2429.
12. Kamat, P. V. Evolution of Perovskite Photovoltaics and Decrease in Energy Payback Time. *J. Phys. Chem. Lett.* **2013**, *4*, 3733–3734.
13. Bisquert, J. The Swift Surge of Perovskite Photovoltaics. *J. Phys. Chem. Lett.* **2013**, *4*, 2597–2598.
14. Snaith, H. J. Perovskites: The Emergence of a New Era for Low-Cost, High-Efficiency Solar Cells. *J. Phys. Chem. Lett.* **2013**, *4*, 3623–3630.
15. Kim, H. S.; Sero, I. M.; Pedro, V. G.; Fabregat-Santiago, F.; Juarez-Perez, E. J.; Park, N. G.; Bisquert, J. Mechanism of Carrier Accumulation in Perovskite Thin-Absorber Solar Cells. *Nat. Commun.* **2013**, *4*, 2242.
16. McGehee, M. D. Materials Science: Fast-Track Solar Cells. *Nature* **2013**, *501*, 323–325.
17. Xing, G. C.; Mathews, N.; Sun, S. Y.; Lim, S. S.; Lam, Y. M.; Gratzel, M.; Mhaisalkar, S.; Sum, T. C. Long-Range Balanced Electron- and Hole-Transport Lengths in Organic–Inorganic $CH_3NH_3PbI_3$. *Science* **2013**, *342*, 344–347.
18. Stranks, S. D.; Eperon, G. E.; Grancini, G.; Menelaou, C.; Alcocer, M. J. P.; Leijtens, T.; Herz, L. M.; Petrozza, A.; Snaith, H. J. Electron–Hole Diffusion Lengths Exceeding 1 Micrometer in an Organometal Trihalide Perovskite Absorber. *Science* **2013**, *342*, 341–344.
19. Eperon, G. E.; Burlakov, V. M.; Docampo, P.; Goriely, A.; Snaith, H. J. Morphological Control for High Performance, Solution-Processed Planar Heterojunction Perovskite Solar Cells. *Adv. Funct. Mater.* **2014**, *24*, 151–157.
20. Liu, M.; Johnston, M. B.; Snaith, H. J. Efficient Planar Heterojunction Perovskite Solar Cells by Vapour Deposition. *Nature* **2013**, *501*, 395–398.
21. Kumar, M. H.; Yantara, N.; Dharani, S.; Gratzel, M.; Mhaisalkar, S.; Boix, P. P.; Mathews, N. Flexible, Low-Temperature, Solution Processed ZnO-Based Perovskite Solid State Solar Cells. *Chem. Commun.* **2013**, *49*, 11089–11091.
22. Sun, S. Y.; Salim, T.; Mathews, N.; Duchamp, M.; Boothroyd, C.; Xing, G.; Sum, T. C.; Lam, Y. M. The Origin of High Efficiency in Low-Temperature Solution-Processable Bilayer Organometal Halide Hybrid Solar Cells. *Energy Environ. Sci.* **2014**, *7*, 399–407.
23. Jeng, J. Y.; Chiang, Y. F.; Lee, M. H.; Peng, S. R.; Guo, T. F.; Chen, P.; Wen, T. C. $CH_3NH_3PbI_3$ Perovskite/Fullerene Planar-Heterojunction Hybrid Solar Cells. *Adv. Mater.* **2013**, *25*, 3727–3732.
24. You, J. B.; Zhang, X. W.; Zhang, S. G.; Tan, H. R.; Ying, J.; Yin, Z. G.; Zhu, Q. S.; Chu, P. K. Electroluminescence Behavior of ZnO/Si Heterojunctions: Energy Band Alignment and Interfacial Microstructure. *J. Appl. Phys.* **2010**, *107*, 083701.
25. Laban, W. A.; Etgar, L. Depleted Hole Conductor-Free Lead Halide Iodide Heterojunction Solar Cells. *Energy Environ. Sci.* **2013**, *6*, 3249–3253.
26. You, J. B.; Chen, C. C.; Dou, L. T.; Murase, S.; Duan, H. S.; Hawks, S. A.; Xu, T.; Son, H. J.; Yu, L. P.; Li, G.; *et al.* Metal Oxide Nanoparticles as an Electron-Transport Layer in High-Performance and Stable Inverted Polymer Solar Cells. *Adv. Mater.* **2012**, *24*, 5267–5272.
27. Yu, Z. F.; Raman, A.; Fan, S. H. Fundamental Limit of Nanophotonic Light Trapping in Solar Cells. *Proc. Natl. Acad. Sci. U.S.A.* **2010**, *107*, 17491–17496.
28. Atwater, H. A.; Polman, A. Plasmonics for Improved Photovoltaic Devices. *Nat. Mater.* **2010**, *9*, 205–213.
29. Yang, J.; You, J. B.; Chen, C. C.; Hsu, W. C.; Tan, H. R.; Zhang, X. W.; Hong, Z. R.; Yang, Y. Plasmonic Polymer Tandem Solar Cells. *ACS Nano* **2011**, *5*, 6210–6217.
30. You, J. B.; Li, X. H.; Xie, F. X.; Sha, W. E. I.; Kwong, J. H. W.; Li, G.; Choy, W. C. H.; Yang, Y. Surface Plasmon and Scattering-Enhanced Low-Bandgap Polymer Solar Cell by a Metal Grating Back Electrode. *Adv. Energy Mater.* **2012**, *2*, 1203–1207.
31. Cowan, S. R.; Roy, A.; Heeger, A. J. Recombination in Polymer-Fullerene Bulk Heterojunction Solar Cells. *Phys. Rev. B* **2010**, *82*, 245207.
32. You, J. B.; Dou, L. T.; Yoshimura, K.; Kato, T.; Ohya, K.; Moriarty, T.; Emery, K.; Chen, C. C.; Gao, J.; Li, G.; *et al.* A Polymer Tandem Solar Cell with 10.6% Power Conversion Efficiency. *Nat. Commun.* **2013**, *4*, 1446.
33. Ma, W.; Yang, C.; Gong, X.; Lee, K.; Heeger, A. J. Thermally Stable, Efficient Polymer Solar Cells with Nanoscale Control of the Interpenetrating Network Morphology. *Adv. Funct. Mater.* **2005**, *15*, 1617–1622.
34. Li, G.; Shrotriya, W.; Huang, J. S.; Yao, Y.; Moriarty, T.; Emery, K.; Yang, Y. High-Efficiency Solution Processable Polymer Photovoltaic Cells by Self-Organization of Polymer Blends. *Nat. Mater.* **2005**, *4*, 864–868.
35. Peet, J.; Kim, J. Y.; Coates, N. E.; Ma, W. L.; Moses, D.; Heeger, A. J.; Bazan, G. C. Efficiency Enhancement in Low-Bandgap Polymer Solar Cells by Processing with Alkane Dithiols. *Nat. Mater.* **2007**, *6*, 497–500.
36. Im, J.-H.; Chung, J.; Kim, S.-J.; Park, N.-G. Synthesis, Structure, and Photovoltaic Property of a Nanocrystalline 2H Perovskite-Type Novel Sensitizer $(CH_3CH_2NH_3)PbI_3$. *Nanoscale Res. Lett.* **2012**, *7*, 353.